JOURNAL OF MATERIALS SCIENCE 27 (1992) 4974–4984

# Tensile behaviour of polycrystalline $Ni_3Al$ intermetallic: influence of environment

T. S. SRIVATSAN, S. SRIRAM
*Department of Mechanical Engineering, The University of Akron, Akron, Ohio 44325-3903, USA*

Alloys based on the nickel aluminide intermetallic compound are particularly attractive for a spectrum of applications because of their high strength and resistance to oxidation. The inferior ductility of polycrystalline nickel aluminide intermetallic alloy was improved by controlled microalloying with boron. This important development has engendered considerable scientific interest in the use of this novel engineering material for temperature-critical and environment-sensitive applications. In this study, an attempt has been made to rationalize the influence of environment on the tensile behaviour of polycrystalline $Ni_3Al$ alloy containing boron and zirconium. Slow strain tensile tests were performed on cold-deformed and annealed samples in environments of laboratory air, distilled water, and aqueous 3.5% sodium chloride solution. A comparison of the tensile properties and fracture behaviour of the polycrystalline intermetallic alloy in the different environments is made to highlight the role of environment in tensile behaviour.

## 1. Introduction

Ordered intermetallic compounds constitute a unique class of metallic materials that form long-range ordered crystal structures below their melting points [1]. Several of these compounds have shown promise for replacing conventional nickel-base superalloys. Nickel aluminide, $Ni_3Al$, is one of a series of intermetallic compounds of nickel and aluminium having an $L1_2$-ordered crystal structure. The aluminium atoms are ordered on the face-centred cubic (f.c.c.) lattice sites of a unit cell such that each aluminium atom has only nickel atoms for nearest neighbours, forming an $L1_2$ superlattice structure. Alloys based on $Ni_3Al$ are being considered for a spectrum of elevated-temperature and cryogenic temperature applications such as gas turbines and steam turbines and including components used in corrosive environments (oil and gas wells, chemical process industry, marine environments). They also find use in automotive pistons, turbochargers, valves, aircraft fasteners, dental drills, forging dies, bearings, tubing, casting moulds for aluminium and glass, heating elements for appliances, and gas and oil-well tubular products [1–5].

In spite of several attractive properties, the usefulness of polycrystalline $Ni_3Al$ and its alloys with chromium, molybdenum and other elements has been restricted on account of its brittleness [6]. The grain boundaries of polycrystalline $Ni_3Al$ are inherently fragile [7], resulting in brittle intergranular fracture. This intergranular brittleness is exacerbated by the intergranular segregation of impurities such as sulphur [7]. However, it has been shown that the intrinsically brittle grain boundaries of polycrystalline $Ni_3Al$ promote intergranular failure even when impurity segregation is insignificant [8–10]. The poor ductility of the material in polycrystalline form was also attributed to concurrent and competing influences of

(a) a low cohesive strength of the grain boundaries,
(b) embrittling effects of impurities at the grain boundaries,
(c) a low density of mobile dislocations, and
(d) a tendency to fail by brittle intergranular fracture [11–14].

Aoki and Izumi [8] made the first experimental attempt at improving the ductility of polycrystalline $Ni_3Al$ by controlled microalloying with boron. Subsequently, Liu *et al.* [10] enhanced the tensile elongation of polycrystalline $Ni_3Al$ by over 50%, with virtually 100% transgranular failure, by careful control of bulk boron content, alloy stoichiometry, and thermomechanical treatment. The use of boron as a microalloying addition resulted in an elimination of intergranular brittleness with a concomitant improvement in the room-temperature ductility, due to a change in fracture mode from brittle intergranular to ductile transgranular in smooth tensile specimens. The change in macroscopic fracture mode was attributed to boron enrichment at grain boundaries as revealed by Auger spectroscopy [10, 15–18]. The resultant intermetallic alloy offered high strength and ductility, making it a promising structural material and enhancing the possibility of practical applications [19].

Unlike conventional metallic alloys, the yield strength of $Ni_3Al$ increases substantially rather than



0022–2461 

decreasing with increasing temperature [20–24]. Many properties of the alloy make it an attractive choice for even cryogenic temperature applications such as forging dies, pump impellers and metal–matrix composites. These are

(i) a high yield strength,
(ii) a high work hardening coefficient, and
(iii) relatively lower density, because of the high aluminium content, compared to conventional nickel-base alloys.

Alloy design efforts to enhance strength, particularly at elevated temperatures, resulted in compositional modification by adding zirconium to contribute to strengthening through solid-solution hardening effects [24, 25].

It has been recognized and documented that the mechanical properties of these alloys are strongly influenced by the test environment. While considerable data on ambient-temperature mechanical properties now exist, information on the influence of environment on this material is desirable. The objective of this paper is to document the influence of environment on the tensile properties and fracture behaviour of the polycrystalline $Ni_3Al$ alloy containing zirconium and boron. The fracture behaviour of the alloy is discussed in terms of aggressiveness of the environment and degree of cold deformation.

## 2. Experimental procedure

The material used in this investigation, polycrystalline $Ni_3Al$ containing zirconium and boron, was provided by Oak Ridge National Laboratory, Oak Ridge, Tennessee. The chemical composition of the alloy is listed in Table I. The flat tensile specimens used were punched out of sheets of the polycrystalline material that were cold-worked (rolled) to different degrees of reduction ranging from 11.4 to 61.4%, with the gauge length parallel to the rolling direction. A schematic diagram of the test specimen is shown in Fig. 1; Table II shows the variation of thickness with deformation. Several samples from each cold-worked sheet were annealed in a controlled environment at 1100 °C for 1 h prior to tensile testing.

Metallographic samples were cut from the as-received material in the cold-deformed plus annealed condition. The samples were mounted in bakelite, and wet-ground on 320, 400 and 600 grit silicon carbide (SiC) paper using water as lubricant and then mechanically polished with 1.0 and 0.05 μm alumina-based lubricant. Grain morphology was revealed using an etch comprising a mixture of 20 $H_2O$, 20 $HNO_3$, 10 HF, 20 $H_3PO_4$, 10 acetic acid and 10 HCl (parts by volume). The specimens were etched for 180 s and examined in an optical microscope and photographed using a standard bright-field technique.

Tensile tests were performed at ambient temperature on the test samples in environments of controlled laboratory air (relative humidity of 55%), doubly distilled water, and aqueous 3.5% sodium chloride solution. The sodium chloride solution was prepared using reagent-grade NaCl and doubly distilled water. The surfaces of the tensile samples were ground with 600-grit silicon carbide paper and then mechanically polished to remove all scratches. The tests were performed on a computer-controlled, servo-hydraulic universal test machine at a nominal strain rate of $10^{-5}\,s^{-1}$. The yield stress was measured at 0.2% plastic strain, and the ductility of the tensile test sample was evaluated from the total elongation to failure, that is, total strain to fracture or failure.

An environmental chamber made of Plexiglass, with a watertight seal at its lower end, as shown in Fig. 2, was used to contain the aqueous solutions (distilled water and 3.5% NaCl). To ensure consistency, the test specimens were exposed (immersed) to the aqueous environments for 60 min prior to testing. Prior to each tensile test, the test specimen was sealed in the Plexiglass chamber using silicone grease and allowed to cure for a full 12 h prior to introducing the aqueous solution into the environmental chamber. The aqueous solutions were open to laboratory air and were not deaerated prior to or during an experiment. Care was taken to keep the test specimen completely submerged in the aqueous medium throughout tensile deformation. This was effected by having a chamber whose length was adequate to contain the test specimen as it expanded during deformation.

TABLE I Nominal chemical composition of the nickel aluminide (wt %)

| Al | B | Cr | Fe | Mn | Mo | P | Zr | Si | Ni |
|---|---|---|---|---|---|---|---|---|---|
| 11.12 | 0.044 | 0.046 | 0.450 | 0.024 | 0.002 | 0.002 | 0.78 | 0.03 | Balance |

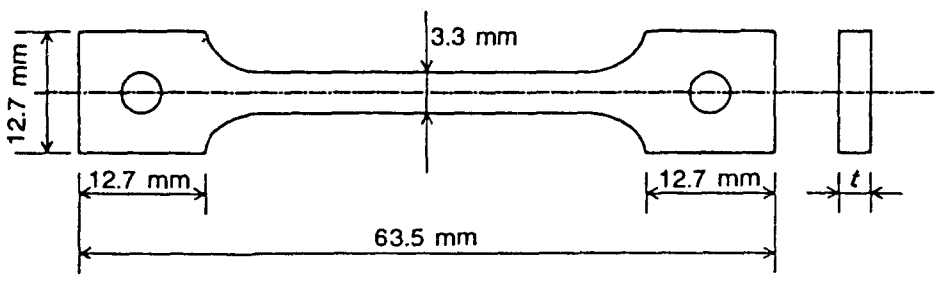


*Figure 1* Schematic diagram showing configuration of test specimen.

TABLE II Variation of test specimen thickness with cold deformation

| Condition | Nominal thickness, $t$ (mm) |
|---|---|
| Undeformed sheet | 1.1176 |
| 11.4% CR | 0.9906 |
| 20.4% CR | 0.889 |
| 27.3% CR | 0.8128 |
| 36.4% CR | 0.7112 |
| 43.2% CR | 0.6350 |
| 47.7% CR | 0.5842 |
| 54.5% CR | 0.508 |
| 58.1% CR | 0.4572 |
| 64.1% CR | 0.4312 |

CR: cold-rolled.

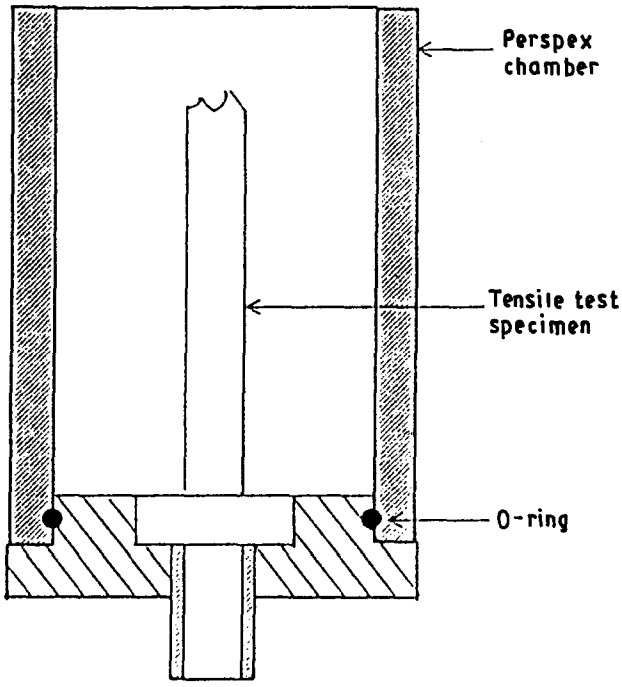


*Figure 2* Environment chamber for testing in aqueous environments.

Fracture surfaces of the deformed tensile samples were examined in a scanning electron microscope (SEM) so as to determine the predominant fracture mode and to characterize the fine-scale fracture features. Samples for SEM observation were obtained from the deformed tensile specimens by sectioning normal to the fracture surface.

## 3. Results and discussion

### 3.1. Initial microstructure

The optical microstructure of the cold-deformed plus annealed material is shown in Fig. 3. Annealing the cold-deformed samples at 1100 °C resulted in a recrystallized microstructure with well-defined grain boundaries. The grain size of the polycrystalline alloy progressively decreased with increasing amount of cold deformation, that is, from 0% (undeformed sheet material) to 61.4% cold-deformed.

### 3.2. Tensile properties

A compilation of the monotonic mechanical properties of the polycrystalline alloy ($Ni_3Al + Zr + B$), cold-worked to various levels and subsequently annealed, is given in Tables III–V below. Duplicate samples were tested for each condition, and no significant variation between the pairs of samples was observed.

#### *3.2.1. Laboratory air environment*

The tensile properties observed in laboratory air are summarized in Table III. The 0.2% offset yield stress and ultimate tensile stress increased with an increase in cold deformation. The maximum strength (yield strength 1061 MPa, ultimate tensile strength 1850 MPa) was achieved for the material that was cold-worked to 54.5%. The observed increase in yield strength and ultimate tensile strength is attributed to intrinsic effects of strain hardening arising from an increase in dislocation density, due to the extrinsic influence of cold deformation on the material. The high strength of the material cold-deformed 54.5%, exemplified in Fig. 4, is quite unique and needs additional verification using an entirely new set of $Ni_3Al + B + Zr$ samples cold-deformed to 54.5% reduction in initial thickness. Fracture of the test samples consistently occurred at the maximum load, and the variation of fracture stress is the same as that of the ultimate tensile stress. The variation of yield strength and ultimate tensile strength for the different conditions is shown in Fig. 4. The elongation to failure showed no observable trend for the test samples that were annealed after prior cold deformation. The variation of elongation to failure for the different conditions was essentially random and well within 10%.

#### *3.2.2. Distilled water*

The tensile properties observed in a distilled water environment are summarized in Table IV. A 50 to 60% degradation in the value of yield strength and over a 50% degradation in ultimate tensile strength are observed when compared with corresponding values in laboratory air. The yield strength was more or less constant for the different degrees or levels of cold deformation. The variation in ultimate tensile strength was random and well within 10% (Fig. 5). Fracture occurred at the maximum load and the variation of fracture stress was similar to that of the ultimate tensile stress. In comparison with results obtained in the less aggressive laboratory air environment, the elongation to failure showed an improvement in the aggressive aqueous environment. The improvement was

(a) as high as 50% for the as-received sheet material, and

(b) as low as 3% for the sheet material cold-worked to 36.4%.

The observed improvement in elongation to failure results from the degradation in strength in the aggressive aqueous environment. The improvement in

TABLE III Monotonic mechanical properties of the polycrystalline $Ni_3Al$ alloy in laboratory air

| Condition | Yield stress (MPa) | Ultimate tensile stress (MPa) | Elongation (%) | Fracture stress (MPa) |
|---|---|---|---|---|
| Undeformed sheet | 362 | 1019 | 30.4 | 1019 |
| 11.4% CR | 408 | 1149 | 33.5 | 1149 |
| 20.4% CR | 424 | 1144 | 33.2 | 1144 |
| 27.4% CR | 481 | 1243 | 31.2 | 1243 |
| 36.4% CR | 493 | 1203 | 31.2 | 1203 |
| 43.2% CR | 615 | 1258 | 28.8 | 1258 |
| 47.7% CR | 668 | 1222 | 32.8 | 1222 |
| 54.5% CR | 1061 | 1850 | 32.8 | 1850 |
| 58.1% CR | 639 | 1420 | 32.8 | 1420 |
| 61.4% CR | 562 | 1295 | 32.8 | 1295 |

Results are means based on two tests at a strain rate of $10^{-5}$ $s^{-1}$; CR: cold-rolled.

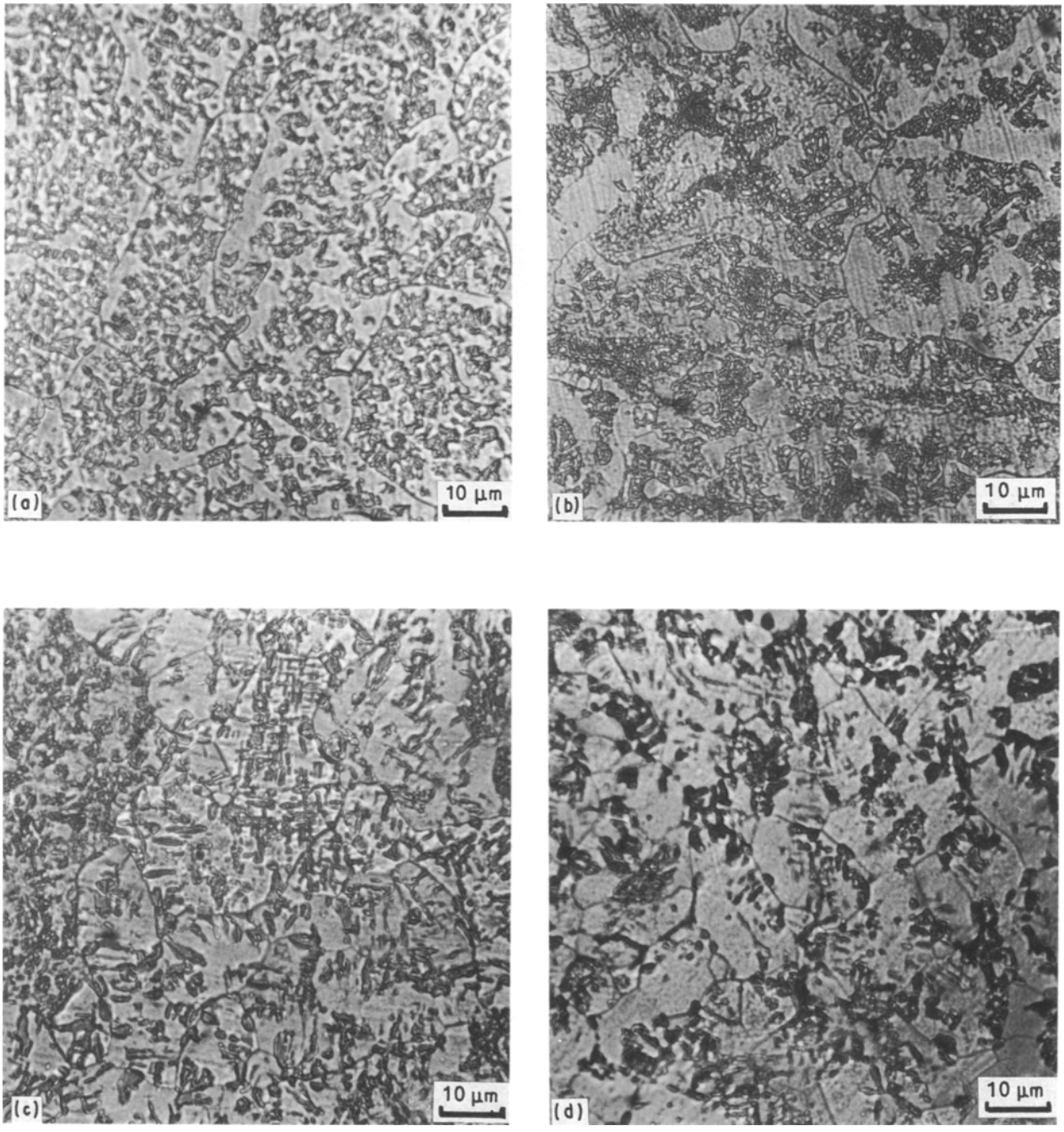


*Figure 3* Optical micrographs of the cold-deformed (cold-rolled) plus annealed polycrystalline $Ni_3Al$ + B intermetallic alloy: (a) undeformed, (b) 11.4%, (c) 27.3%, (d) 36.4%, (e) 47.7%, (f) 54.5%, (g) 59.1%, (h) 61.4%.

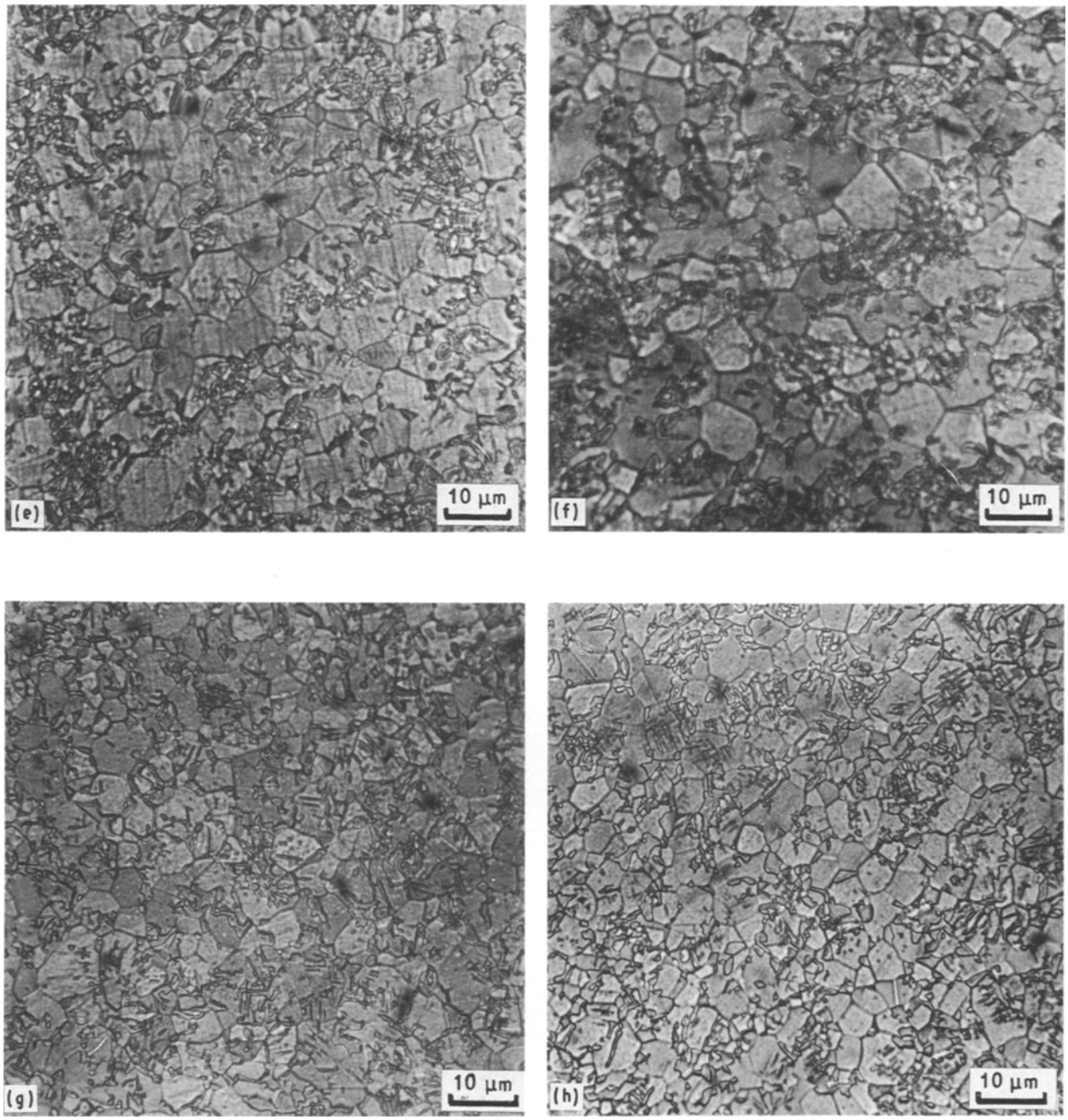


*Figure 3* continued.

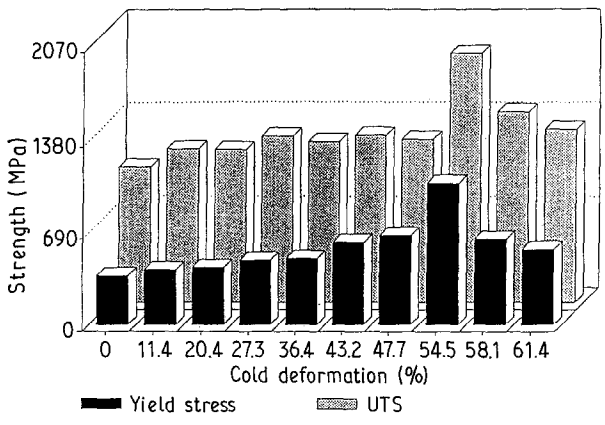


*Figure 4* Variation of yield strength and ultimate tensile strength with degree of cold deformation in laboratory air. Strain rate $10^{-5}\,s^{-1}$.

elongation to failure obscures the reduction or degradation in ductility arising from hydrogen embrittlement and other environmental effects. The small section size (thickness) of the test sample (Fig. 1) apparently provided for a larger influence of environment on the load-carrying capability of the material than for a detrimental influence of environment on ductility. The engineering stress–engineering strain curves (Fig. 6) reveal an increase in cold deformation to result in an increase in strength, due to intrinsic effects of strain hardening, but with a concomitant loss in ductility.

### 3.2.3. 3.5% sodium chloride solution

The properties in an aggressive aqueous sodium chloride environment, summarized in Table V, reveal the

TABLE IV Monotonic mechanical properties of the polycrystalline $Ni_3Al$ alloy in distilled water

| Condition | Yield stress (MPa) | Ultimate tensile stress (MPa) | Elongation (%) | Fracture stress (MPa) |
|---|---|---|---|---|
| Undeformed sheet | 210 | 526 | 44.6 | 526 |
| 11.4% CR | 214 | 574 | 43.0 | 574 |
| 20.4% CR | 236 | 580 | 38.2 | 580 |
| 27.4% CR | 240 | 603 | 37.7 | 603 |
| 36.4% CR | 212 | 560 | 32.0 | 560 |
| 43.2% CR | 242 | 602 | 40.1 | 602 |
| 47.7% CR | 236 | 588 | 37.4 | 588 |
| 54.5% CR | 253 | 610 | 41.6 | 610 |
| 58.1% CR | 257 | 610 | 41.1 | 610 |
| 61.4% CR | 254 | 609 | 41.1 | 609 |

Results are means based on two tests at a strain rate of $10^{-5}\ s^{-1}$; CR: cold-rolled.

TABLE V Monotonic mechanical properties of the polycrystalline intermetallic in 3.5% sodium chloride solution

| Condition | Yield stress (MPa) | Ultimate tensile stress (MPa) | Elongation (%) | Fracture stress (MPa) |
|---|---|---|---|---|
| Undeformed sheet | 182 | 518 | 52.8 | 518 |
| 11.4% CR | 196 | 563 | 42.9 | 563 |
| 20.4% CR | 186 | 566 | 37.4 | 566 |
| 27.4% CR | 212 | 599 | 35.7 | 599 |
| 36.4% CR | 202 | 615 | 41.0 | 615 |
| 43.2% CR | 243 | 624 | 41.1 | 624 |
| 47.7% CR | 216 | 622 | 42.7 | 622 |
| 54.5% CR | 265 | 640 | 41.0 | 640 |
| 58.1% CR | 258 | 561 | 39.1 | 561 |
| 61.4% CR | 263 | 623 | 41.0 | 623 |

Results are means based on two tests at a strain rate of $10^{-5}\ s^{-1}$; CR: cold-rolled.

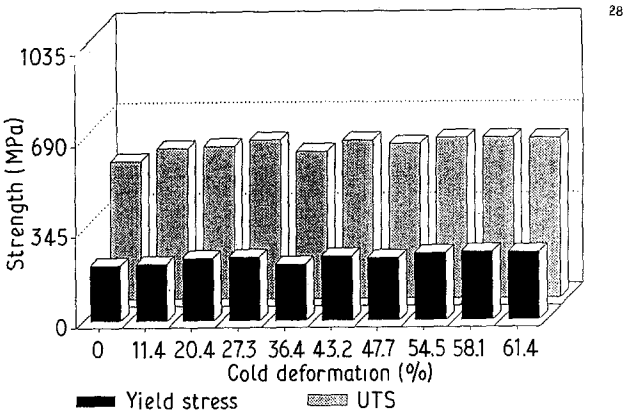


*Figure 5* Variation of yield strength and ultimate tensile strength with degree of cold deformation in distilled water. Strain rate $10^{-5}\ s^{-1}$.

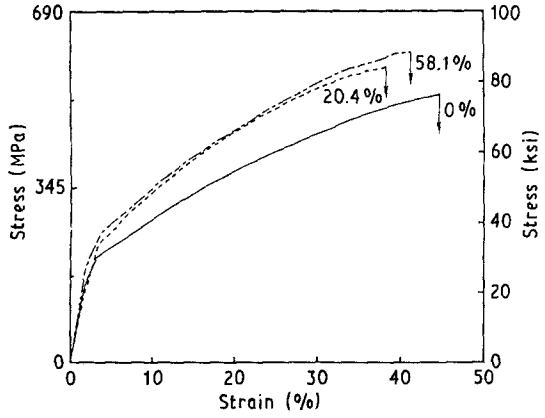


*Figure 6* Comparison of engineering stress–engineering strain curves for the polycrystalline alloy deformed at $10^{-5}\ s^{-1}$ in distilled water.

yield strength of the polycrystalline alloy to be 50% lower than the corresponding value in laboratory air (Table III). For the different levels/degrees of cold deformation, a degradation in ultimate tensile strength compared to corresponding values in laboratory air was also evident. The degradation was as high as 60% for the polycrystalline alloy cold-deformed to 54.5%. With fracture occurring at or near the maximum load, the fracture stress followed a similar trend as the ultimate strength. The variation of strength (yield strength and ultimate tensile strength) for the different conditions is shown in Fig. 7.

As in the environments of laboratory air and distilled water, the elongation to failure showed no observable trend with increasing cold deformation given to the as-received sheet material. The elongation to failure values in aqueous sodium chloride solution showed an actual improvement over corresponding values in laboratory air. The improvement was in the range of 10–60%. However, an improvement in elongation in aqueous NaCl was in the range of 10–30% over corresponding values in distilled water. A comparison of elongation to failure, for the different cold-deformed conditions, in the three environments is made in Fig. 8. The ratio of strain to failure in the aqueous environments of NaCl and distilled water with respect to strain to failure in laboratory air is provided in Fig. 9. This figure reveals an improvement

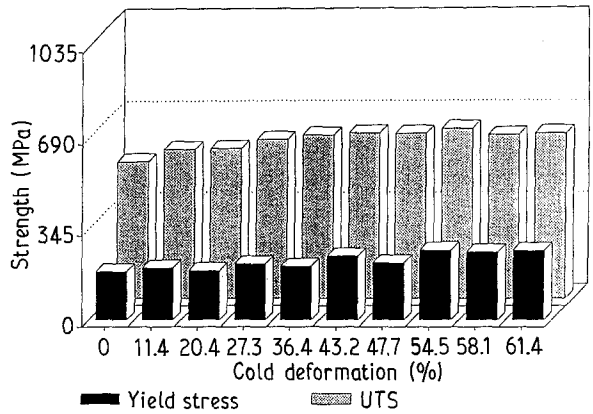


*Figure 7* Variation of yield strength and ultimate tensile strength for samples deformed to failure in 3.5% NaCl solution. Strain rate $10^{-5}\,s^{-1}$.

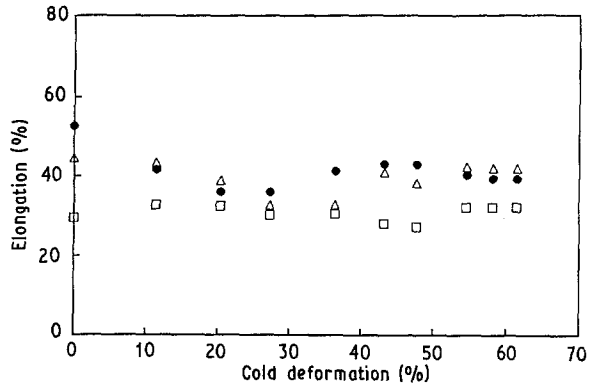


*Figure 8* Comparison of elongation-to-failure for the polycrystalline $Ni_3Al$ alloy in the three environments. (□) Laboratory air, (△) distilled water and (●) 3.5% NaCl solution.

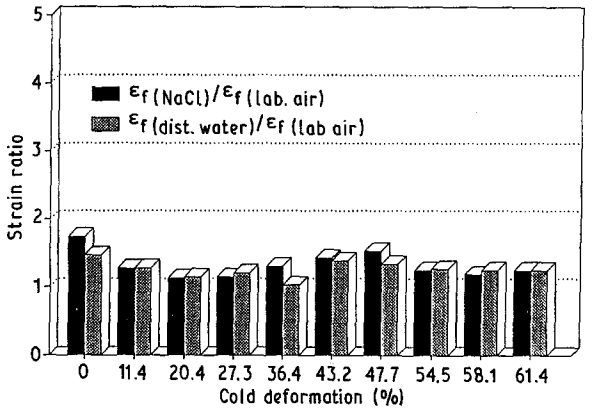


*Figure 9* Effect of environment on elongation-to-failure ratio of the polycrystalline $Ni_3Al$ alloy.

in strain-to-failure in the aggressive aqueous environments in comparison with laboratory air. The improvement in elongation-to-failure or strain-to-failure is consistent with the loss in strength experienced by the polycrystalline intermetallic alloy in the aggressive environments.

## 3.3. Fracture behaviour and deformation characteristics

The tensile fracture surfaces are helpful in elucidating

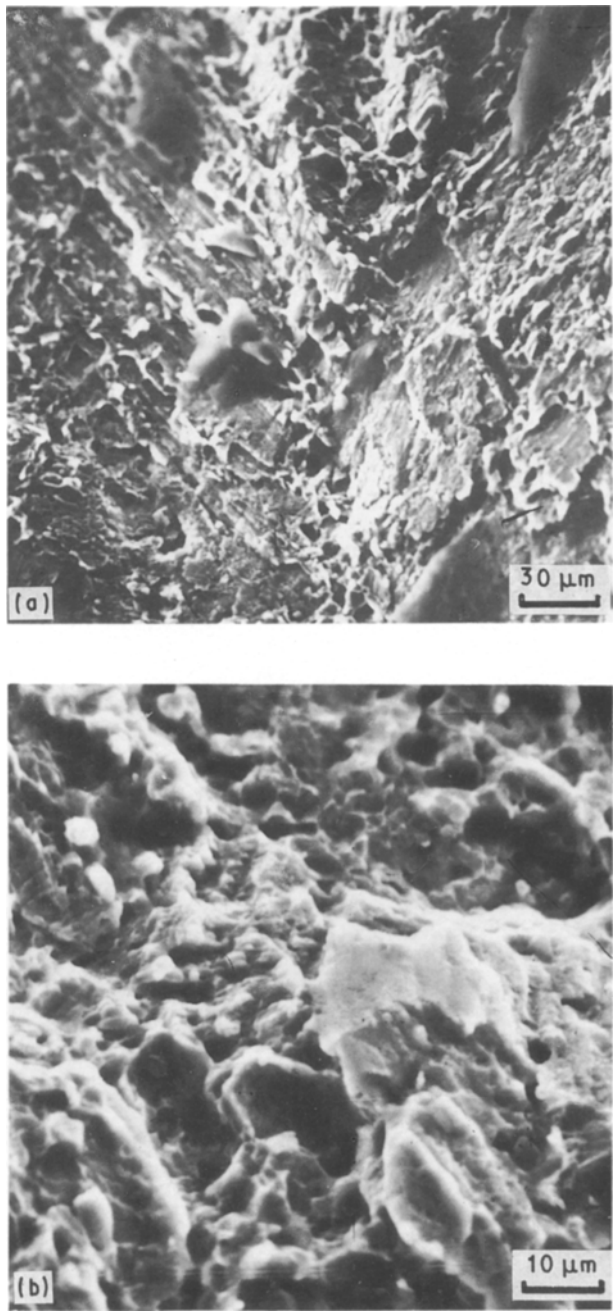


*Figure 10* Scanning electron micrographs showing fracture surface features of the undeformed plus annealed tensile sample deformed in laboratory air: (a) transgranular fracture, (b) voids on transgranular fracture surface.

microstructural effects on ductility and fracture properties of the polycrystalline $Ni_3Al$ alloy. SEM examination of the fracture surface features of the deformed tensile specimens was done at low magnification to identify the overall fracture morphology, and at higher magnification to identify the fine-scale fracture features. Fractography of the tensile samples revealed different features in the different environments. Representative fracture features for samples deformed to failure in the different environments are shown in Figs 10–13.

On a macroscopic scale, tensile fracture in a laboratory air environment was transgranular for the as-received material (annealed undeformed sheet) as shown in Fig. 10a. Examination of the fracture surface at higher magnification revealed fine microscopic

voids randomly distributed across the fracture surface (Fig. 10b). The area between voids was covered with shallow dimples.

Tensile fracture of the samples that were cold-deformed to 61.4% and annealed was quite different from that of the as-received sheet material (annealed undeformed sheet). Fracture of the cold-deformed samples was bimodal with evidence of traces of intergranular cracking (Fig. 11a). Examination of the fracture surfaces at higher magnification revealed macroscopic voids intermingled with numerous microscopic voids, indicating ductile failure (Fig. 11b). Shallow near-equiaxed dimples were found adjacent to the intergranular fracture surface (Fig. 11c). During tensile deformation the progressive build-up of dislocations on the slip band eventually results in stress concentration at the point of impingement of the slip band on the grain boundary regions. The localized deformation and resultant high stress concentration facilitates the nucleation of voids at the inclusions and impurities along the grain boundaries. The fine microvoids coalesce, and the halves of these voids are the shallow dimples observed on the fracture surface.

In the doubly distilled water environment, fracture of the polycrystalline alloy that was cold-deformed to 61.4% and annealed was mixed intergranular and transgranular (bimodal) with a population of voids spread throughout the transgranular regions. Corrosion deposits were few and isolated and covered sections of the fracture surface (Fig. 12). The scales of corrosion deposit revealed cracking at selected regions.

In the aqueous 3.5% NaCl solution fracture surfaces of the polycrystalline alloy were found to be covered with large-scale corrosion deposits. The surface regions that were devoid of corrosion deposits revealed mixed intergranular and transgranular failure (Fig. 13a). Large macroscopic voids were found distributed at random on the transgranular fracture surface. At higher magnification, few shallow dimples were found covering the transgranular fracture regions (Fig. 13b).

In earlier studies [26], polycrystalline nickel aluminide ($Ni_3Al$) was found to be brittle and the alloy failed intergranularly, displaying limited ductility. However, recent advances in processing such as microalloying with boron have resulted in an $Ni_3Al$ intermetallic compound displaying a ductile mode of failure. Boron segregates to grain boundaries of the polycrystalline intermetallic compound [10, 27]. The effect of boron appears to be a strengthening of the grain boundary so that it can withstand the stresses introduced by planar deformation bands (Fig. 14). Planar slip deformation is characteristic of intermetallics and ordered alloys where the superlattice dislocations can be visualized as two unit dislocations that move together, separated by a strip of antiphase

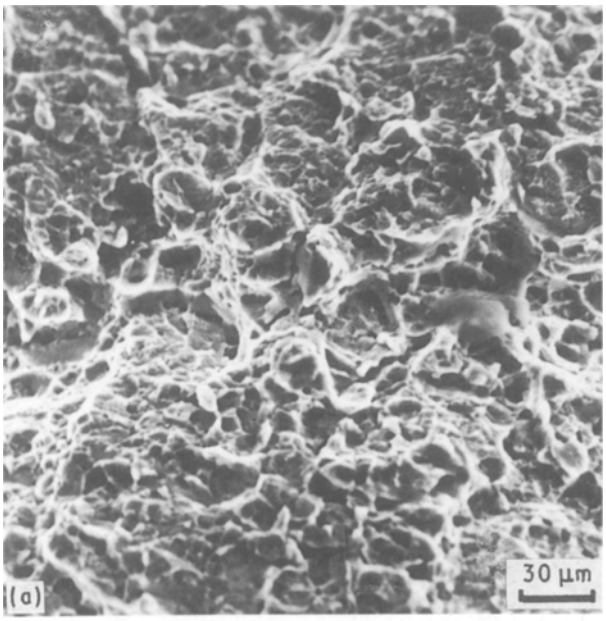


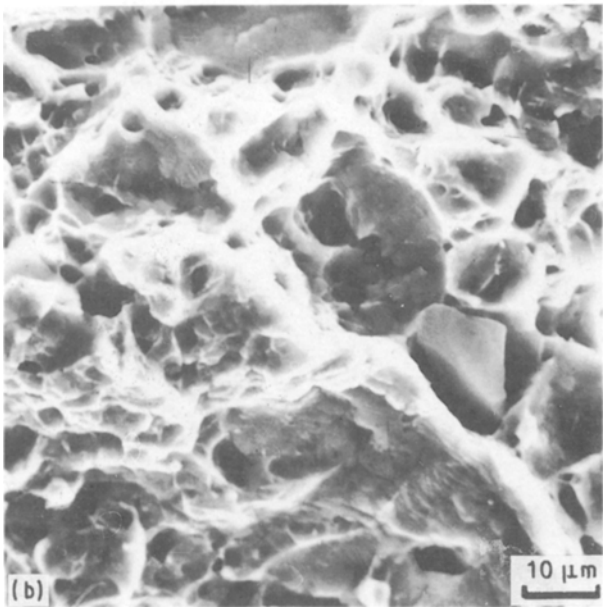


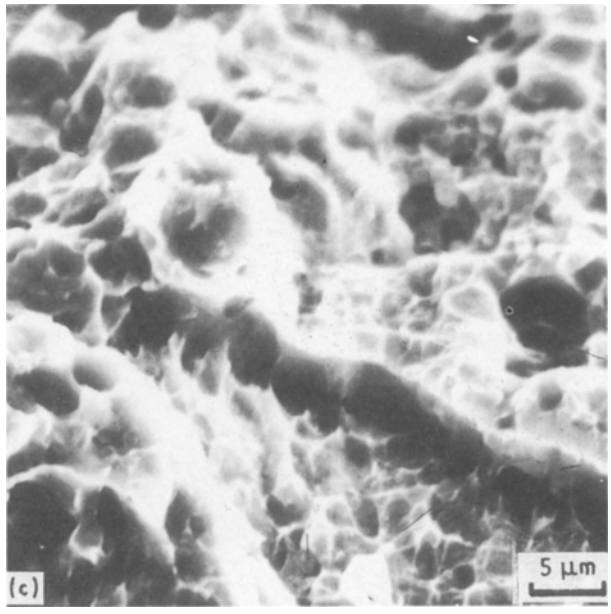


*Figure 11* Scanning electron micrographs showing fracture surface features of samples cold-deformed to 61.4% plus annealed and deformed to failure in laboratory air: (a) intergranular cracking, (b) ductile failure, (c) shallow near-equiaxed dimples.

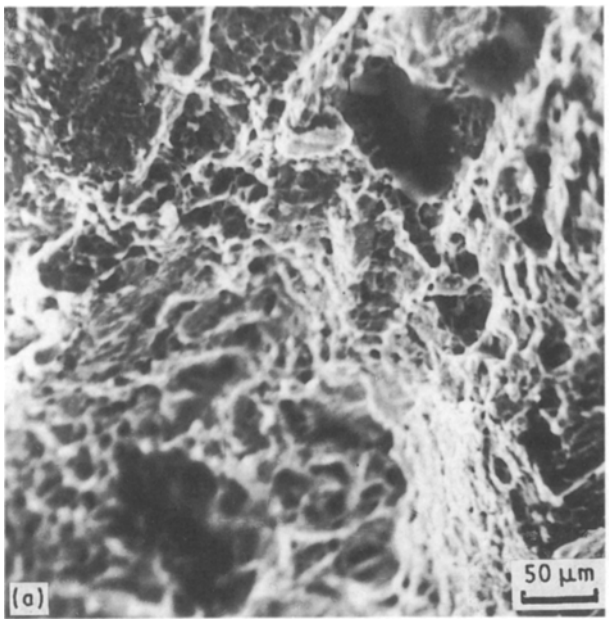


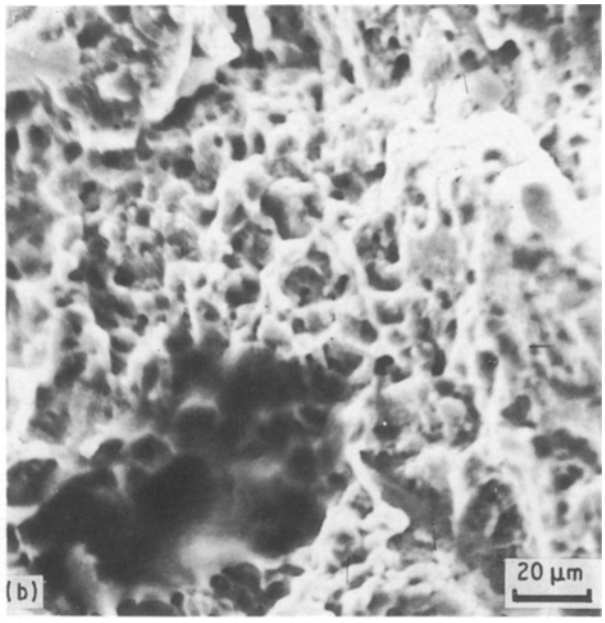


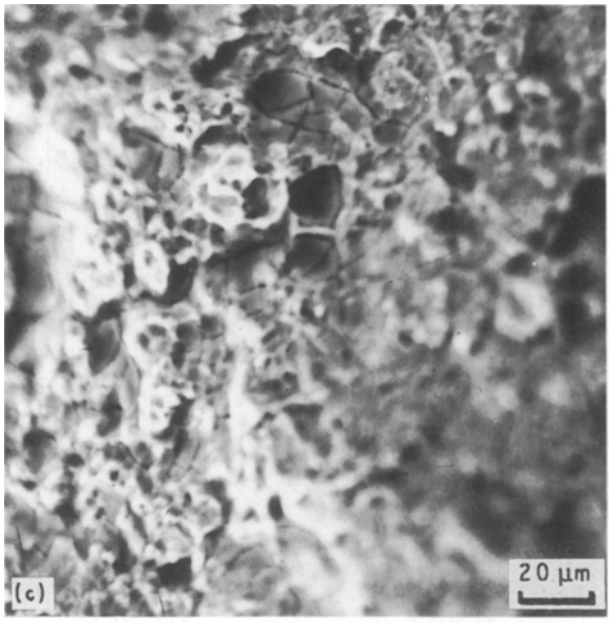


*Figure 12* Scanning electron micrographs of 61.4% cold-deformed plus annealed samples deformed to failure in distilled water. (a) General morphology, (b) corrosion deposit, (c) cracking at corrosion deposit.

boundary [28, 29]. This dislocation structure restricts cross-slip and thus there exists a lesser likelihood of accommodating slip processes at the grain boundary as dislocations progressively pile up. An intensive examination of the polished surfaces of the deformed tensile specimens revealed arrays of planar deformation bands indicative of the ductility of the material. The number and intensity of the deformation bands was observed to be more for the undeformed, 11.4 and 20.4% cold-deformed samples (Fig. 14) than for the samples that were cold-deformed to greater reductions in thickness (61.4%). The observation of decreased planar slip deformation, with increased cold deformation is consistent with the observed loss in tensile

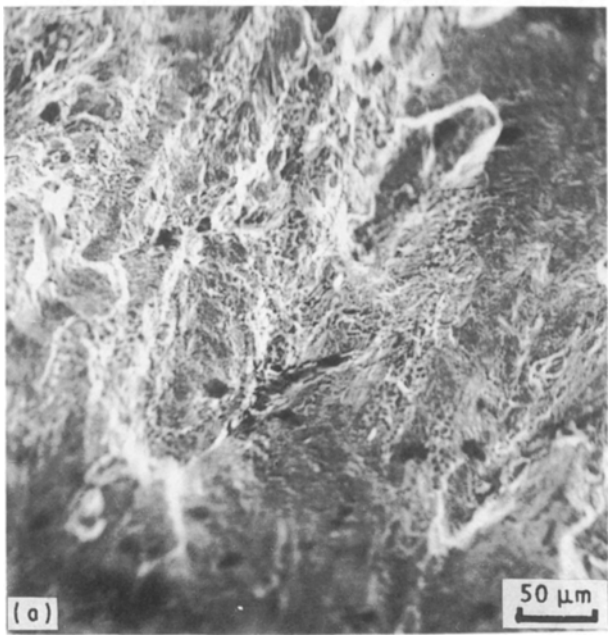


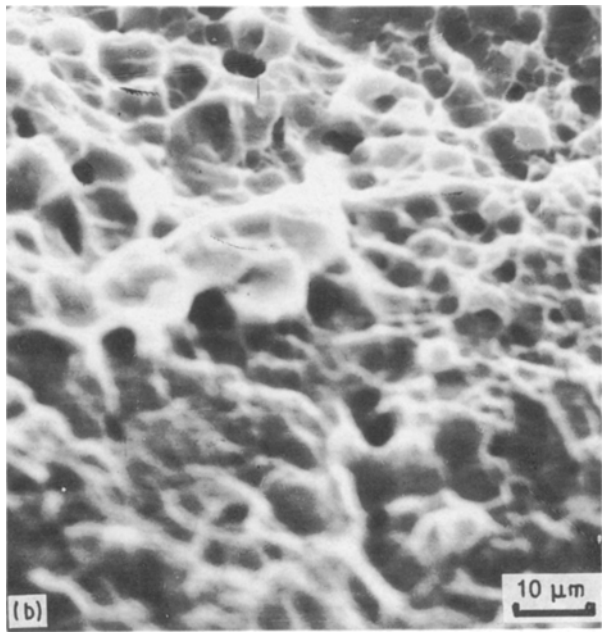


*Figure 13* Scanning electron micrographs of 61.4% cold-deformed plus annealed samples deformed to failure in 3.5% sodium chloride solution: (a) mixed transgranular and intergranular failure, (b) shallow dimples on transgranular fracture surface.

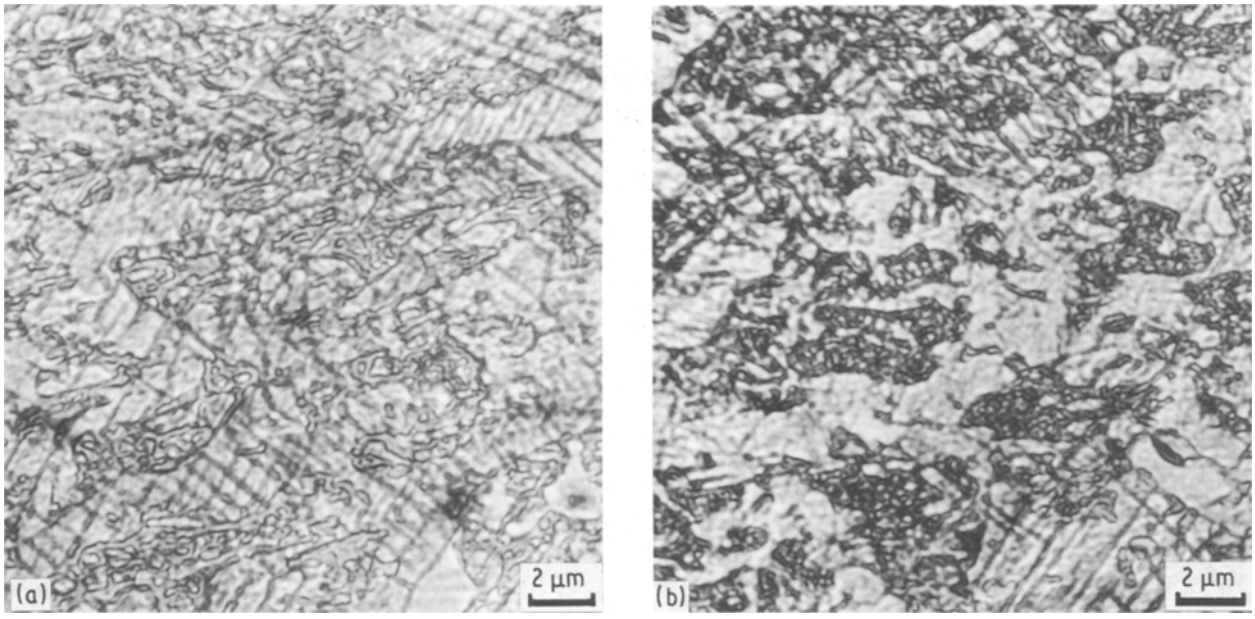


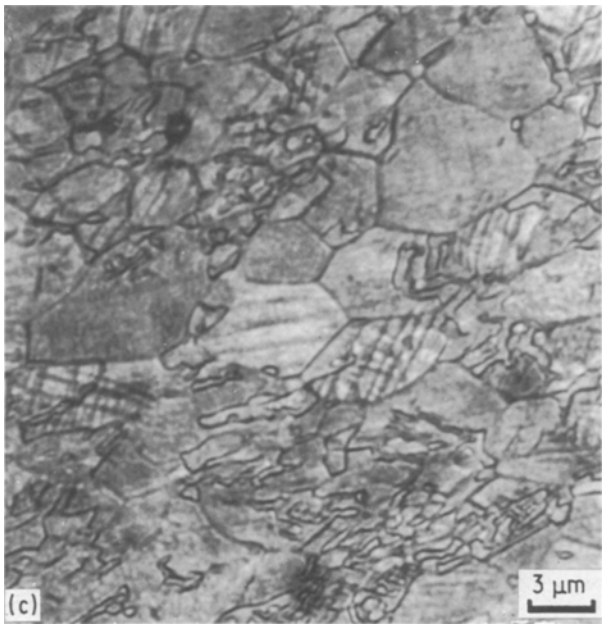


*Figure 14* Optical micrographs of polished surface of test specimen showing planar deformation bands: (a) undeformed material, (b) 20.4% cold-deformed, (c) 61.4% cold-deformed.

ductility with an increase in degree of cold deformation imparted to the polycrystalline intermetallic alloy.

The pile-up of dislocations on the slip band culminates in stress concentration at the grain boundary. It seems likely that a build-up of stress at grain boundaries, coupled with the presence of hydrogen from the aqueous environment, promotes embrittlement [30] and ensuing intergranular fracture when the concentrated stress at a grain boundary exceeds the cohesive strength of the boundaries. It seems plausible that the intergranular fracture observed in aqueous 3.5% sodium chloride solution is exacerbated by the formation and presence of corrosion deposits. The short duration of the tensile test seems to be insufficient to provide a protective oxide layer throughout the sample surface. The intergranular regions appear to be the result of hydrogen penetration through the layer of corrosion deposit, which could be due to either a lack of uniformity or insufficient thickness.

An intensive examination of the fracture surfaces of samples of the polycrystalline intermetallic compound deformed to failure in the aggressive aqueous environments was hindered by the presence of corrosion deposits.

## 4. Conclusions

Based on a study of the influence of environment on room-temperature tensile behaviour of the polycrystalline $Ni_3Al$ alloy containing zirconium and boron, the following observations are made:

1. The strength of the polycrystalline alloy degraded in aggressive aqueous environments with respect to laboratory air was observed. The degradation in strength was as high as 60% and occurred for both the as-received sheet material and for the cold-deformed conditions. The degradation is attributed to the marked influence of environment on the small cross-sectional size of the test specimen, resulting in a concomitant influence on the load-carrying capability of the test specimen.
2. The elongation to failure improved in the aggressive aqueous environments over corresponding values in laboratory air. The improvement varied in the range from 10 to 60%.
3. Tensile fracture of the polycrystalline alloy in laboratory air was predominantly transgranular for the as-received undeformed sheet material and for the cold-deformed conditions, with both macroscopic and fine microscopic voids dispersed on the fracture surface.
4. Fracture in the aqueous distilled water and 3.5% sodium chloride environments was mixed-mode with evidence of intergranular cracking. The fracture surfaces were covered with corrosion deposits.

5. The stress concentration at grain boundaries due to planar slip deformation, exacerbated by the presence of an aggressive environment, is a plausible cause for hydrogen embrittlement and grain boundary attack of the polycrystalline $Ni_3Al + B$ intermetallic alloy.

## Acknowledgements

The present study was partially supported by the state of Ohio: Board of Regents under Grant No. 5-34026. Material used in this study was provided by Oak Ridge National Laboratory, Oak Ridge, Tennessee. Thanks are due to Dr Vinod K. Sikka (Program Manager) for his encouragement and for his help in procuring the material.

## References

1. C. T. LIU and J. O. STIEGLER, *Science* **221** (1984) 636.
2. V. K. SIKKA and E. A. LORIA, in Proceedings of International Symposium on Nickel Metallurgy, CIM, Warrendale, Pennsylvania Vol. 2 (1986) p. 293.
3. V. K. SIKKA, C. T. LIU and E. A. LORIA, in Proceedings, "Structural Metals by Rapid Solidification" (American Society for Metals, Metals Park, Ohio, 1987) p. 417.
4. C. T. LIU, in "MICON 86", ASTM STP 979 (American Society for Testing and Materials, Philadelphia, 1988) pp. 222–227.
5. U. BERTOCCI, J. L. FINK, D. E. HALL, P. V. MADSEN and R. E. RICKER, *Corros. Sci.* **31** (1990) 471.
6. A. CHOUDHURY, C. L. WHITE and C. R. BROOKS, "The Effect of Thermal History on Intergranular Boron Segregation and Fracture Morphology of $Ni_3Al$", Final Report (Oak Ridge National Laboratory, Oak Ridge, Tennessee, 1987)
7. C. L. WHITE and D. F. STEIN, *Metall. Trans.* **9A** (1978) 13.
8. K. AOKI and O. IZUMI, *Nippon Kinzoku Gakkuishi* **43** (1979) 1190.
9. T. Y. OGURA, S. HANADA, J. MASUMOTO and O. IZUMI, *Metall. Trans.* **16A** (1985) 411.
10. C. T. LIU, C. L. WHITE and J. A. HORTON, *Acta Metall.* **33** (1985) 213.
11. G. W. GROVES and A. KELLY, *Phil. Mag.* **8** (1963) 877.
12. E. GRALA, in "Mechanical Properties of Intermetallic Compounds", edited by J. H. Westbrook (Wiley, New York, 1960) pp. 638–648.
13. S. V. RAJ, R. D. NOEBE and R. BOWMAN, *Scripta Metall.* **23** (1989) 2049.
14. C. T. LIU, *Mater. Res. Soc. Symp. Proc.* **81** (1987) 355.
15. P. S. KHADILKAR, J. J. LEWANDOWSKI and K. VEDULA, *Metall. Trans.* **20A** (1989) 1247.
16. N. MASAHASHI, T. TAKASUGI and O. IZUMI, *Acta Metall.* **36** (1988) 1823.
17. C. T. LIU and C. L. WHITE, *ibid.* **35** (1987) 643.
18. C. L. WHITE, R. A. PADGETT, C. T. LIU and S. M. YABISOVE, *Scripta Metall.* **18** (1984) 1417.
19. A. CHOUDHURY, C. L. WHITE and C. R. BROOKS, *ibid.* **20** (1986) 1061.
20. P. A. FLINN, *Trans. TMS-AIME* **218** (1960) 145.
21. R. G. DAVIES and N. S. STOLOFF, *ibid.* **233** (1965) 714.
22. E. A. AITKEN, "Intermetallic Compounds" (Wiley Interscience, New York, 1967) p. 491.
23. P. H. THORTON, R. G. DAVIS and T. L. JOHNSON, *Metall. Trans.* **1** (1970) 207.
24. C. T. LIU and V. K. SIKKA, *J. Metals* **38**(5) (1986) 19.
25. V. K. SIKKA, *Adv. Mater. Manuf. Process.* **4**(1) (1988) 1.
26. R. W. GUARD and J. H. WESTBROOK, *Trans. Met. Soc. AIME* **215** (1959) 807.
27. C. T. LIU, C. C. WHITE, C. C. KOCH and E. H. LEE, in "High Temperature Materials Chemistry II", edited by Z. A. Munir and D. Cubicciotti (Electrochemical Society inc, 1983) pp. 32–42.
28. A. K. KURUVILLA and N. S. STOLOFF, *Scripta Metall.* **19** (1985) 83.
29. S. HANADA, S. WATANABE and O. IZUMI, *J. Mater. Sci.* **21** (1986) 203.
30. R. E. RICKER, D. E. HALL and J. L. FINK, *Scripta Metall. Mater.* **24** (1990) 291.

*Received 17 May*
*and accepted 27 September 1991*